PCCP

RSC Publishing

PAPER

View Article Online
View Journal | View Issue

Cite this: *Phys. Chem. Chem. Phys.*, 2013, **15**, 19360

The effect of fluorine substitution on chiral recognition: interplay of CH···π, OH···π and CH···F interactions in gas-phase complexes of 1-aryl-1-ethanol with butan-2-ol†

Alessandra Ciavardini,[ab] Flaminia Rondino,[c] Alessandra Paladini,[d] Maurizio Speranza,[b] Simonetta Fornarini,[b] Mauro Satta*[e] and Susanna Piccirillo*[a]

Received 30th July 2013,
Accepted 18th September 2013

DOI: 10.1039/c3cp53215a

www.rsc.org/pccp

The molecular diastereomeric complexes between *R*-1-phenyl-1-ethanol, *S*-1-(4-fluorophenyl)ethanol and *S*-1-(2-fluorophenyl)ethanol and *R* and *S*-butan-2-ol, isolated under molecular beam conditions in the gas phase, have been investigated by mass-selective resonant two-photon ionization (R2PI) and infrared depleted R2PI (IR-R2PI). The comparison of the three systems allowed us to highlight the significance of specific intermolecular interactions in the chiral discrimination process. The interpretation of the results is based on theoretical predictions mainly at the D-B3LYP/6-31++G** level of theory. The homo and heterochiral complexes are endowed with fine differences in intermolecular interactions, namely strong OH···O, and weaker CH···π, OH···π, CH···F as well as repulsive interactions. The presence of a fluorine atom in the *para* position of the aromatic ring does not influence the overall geometry of the complex whilst it affects the electron density in the π system and the strength of CH···π and OH···π interactions. The role and the importance of CH···F intermolecular interactions are evident in the complexes with fluorine substitution in the *ortho* position. While the *ortho* hetero complex is structurally analogous to the hetero *para* and non-fluorinated structures, butan-2-ol in the *ortho* homo adduct adopts a different conformation in order to establish a CH···F intermolecular interaction.

1. Introduction

Chirality is an essential element of life either at the molecular or at the supramolecular level. The transmission of chiral information, the recognition properties as well as the functionality of biomolecules rely substantially on non-covalent intra and intermolecular interactions and their study is of fundamental interest and has a deep impact on chemistry, biology, pharmacology, materials science and even astrophysics. In combination with stronger non-covalent interactions with high directionality, such as hydrogen bonding or metal coordination, π···π stacking forces and very weak XH···π (X = O, N and C) or CH···X interactions may also play an essential role in chiral discrimination processes.[1] In the last few years many efforts have been directed to explore the potential of weaker non-covalent forces in stabilizing specific molecular conformations or molecular assemblies involving chiral molecules. In this context, fluorine substitution[2] is a widely utilized approach, because it can endow novel interactions, such as CH···F or OH···F interactions, which however still remain largely uncharacterized in molecular complexes. A large number of therapeutic and diagnostic agents contain strategically placed fluorine atoms which also allow simultaneous modulation of electronic and lipophilic parameters and affect binding affinity and relevant pharmacokinetic properties.

In order to disentangle the various contributions to chiral discrimination in molecular aggregates, thermodynamic parameters as well as the kinetic consequences of stereospecific interactions must be taken into account. Among the questions that must be addressed are (i) which are the intermolecular forces responsible for holding chiral molecules together, (ii) which subtle combination of interactions is responsible for enantioselective binding, (iii) which are the consequences of

[a] *Dip. di Scienze e Tecnologie Chimiche, Università di Roma "Tor Vergata", via della Ricerca Scientifica, 00133 Rome, Italy. E-mail: piccirillo@fisica.uniroma2.it*
[b] *Dip.di Chimica e Tecnologie del Farmaco, Università di Roma "La Sapienza", Rome, Italy*
[c] *C.R ENEA Frascati, Via E. Fermi 45, 00044 Frascati, Roma, Italy*
[d] *CNR – IMIP, Area della Ricerca di Roma 1, Monterotondo Scalo, Italy*
[e] *CNR-ISMN, Rome, Italy*

† Electronic supplementary information (ESI) available. See DOI: 10.1039/c3cp53215a

stereospecific interactions on the dynamics of relevant reactive processes.

A convenient approach to gain insight into these questions is to investigate non-covalent complexes at the molecular level in the isolated state, making use of appropriate spectroscopic techniques.[3] Gas phase experiments and quantum chemical modeling can allow us to understand in detail the structural and energetic factors underlying chiral selectivity. Besides, it has been recognized that in complexes in solution, often molecules are extensively desolvated at active interaction sites. Hence, a proper evaluation of gas phase interactions allows also a subsequent reasonable determination of the effect of solvent firstly in hydrated complexes and then in solution.[4]

Much effort has been invested in recent years into the study of chiral discrimination in molecular complexes in the gas phase, utilizing several spectroscopic techniques,[5–9] and/or theoretical means.[10–12] Among the numerous examined systems, the adducts between *R*-1-phenyl-ethanol (E_R, Fig. 1) and *R* or *S* butan-2-ol have been largely studied[13–17] using resonant two photon ionization (R2PI) spectroscopy: they represent one of the simpler model systems for the study of chiral discrimination between aromatic–aliphatic molecules bound by a single hydrogen bond. By means of R2PI investigations it was ascertained that the binding energy difference between the RR and RS complexes is in the 0.7–1.0 kcal mol^{-1} range,[14–16] with the RR complex more stable than the RS complex. It has also been pointed out that besides the main electrostatic interaction between the partners (hydrogen bond), interactions with the π-system play an important role and are probably responsible for chiral recognition in these systems.

We report here the results of the first comparative study in which we have investigated in detail the effect of stereospecific interactions in the presence of a fluorine atom on the aromatic ring of *R*-1-phenyl-1-ethanol. Specifically we present new R2PI spectroscopic data for the gas phase complexes between *R* and *S*-butan-2-ol and (*S*)-1-(2-fluorophenyl)ethanol (oFE_S, Fig. 1), together with a summary of the main findings obtained in previous studies on the adducts of *R* and *S*-butan-2-ol with *S*-1-(4-fluorophenyl)ethanol (pFE_S)[18] and *R*-1-phenyl1-ethanol (E_R) (Fig. 1).[13]

Our aim is to characterize and compare the conformations of the complexes and to figure out whether and how the substitution of the F atom in the *para*- and *ortho*-position controls the chiral discrimination process.

For consistency purposes within this paper, it is convenient to define the diastereoisomeric complexes between the chiral aromatic chromophores (oFE_S, pFE_S and E_R) and the two enantiomers of butan-2-ol (B_R and B_S) as "homochiral" or "homo" when the chromophore and the partner have the same configuration (*i.e.* $oFE_S{\cdot}B_S$), and "heterochiral" or "hetero" in the opposite case (*i.e.* $E_R{\cdot}B_S$). Because of the stereospecificity of the chromophore–solvent interactions, the hetero and homochiral diastereomeric pairs display specific spectroscopic signatures, namely, the electronic band origin of each pair, their vibronic bands and their dissociation thresholds. Additional data for the spectroscopic identification of these complexes are obtained by the use of the IR-R2PI double resonance technique.

The interpretation of the experimental results and the comparison between the different systems have been performed in light of a quantum mechanical study for all the above-quoted systems. The methods used are Dispersion-Corrected Density Functional Theory with the B3LYP functional (D-B3LYP) as well as second-order Møller–Plesset theory (MP2).

Our combined experimental–computational approach gives answers that help in understanding, at a molecular level, the influence of specific CH···π, OH···π and CH···F interactions in relation to the molecular and chiral recognition processes in these model systems.

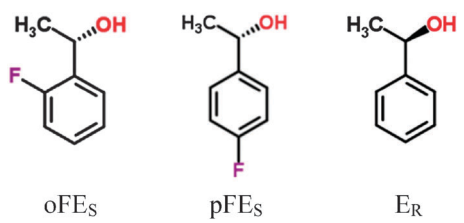

Fig. 1 Structures of: *S*-1-(2-fluorophenyl)ethanol (oFE_S), *S*-1-(4-fluorophenyl)-ethanol (pFE_S) and *R*-1-phenyl-1-ethanol (E_R).

2. Methodology

2.1 Experimental section

Details of the experimental setup for the R2PI- and IR/R2PI-spectroscopies have already been published elsewhere.[18,19] Briefly, clusters containing one stereoisomer of the aromatic chromophore with either *R* or *S*-2-butanol are produced in a 10 Hz-pulsed seeded supersonic expansion of their vapors, generated in temperature-controlled reservoirs (50 °C and 0 °C respectively) using argon as carrier gas at a backing pressure of 2 bar. The 1 : 1 clusters are ionized *via* one-color R2PI utilizing the frequency of a Nd:YAG-pumped pulsed dye laser with associated crystals for nonlinear optical conversion. The photoions are mass analyzed in a time-of-flight mass spectrometer and detected using a channeltron. The signal is averaged using a digital oscilloscope and stored on a PC. The R2PI spectrum of a particular species is recorded by monitoring its ion yield in the mass spectrum as a function of the laser wavelength. Due to the resonant step in the two photon ionization process, the signal variation represents the UV excitation spectrum of the neutral precursor. The spectra of the non-covalent diastereomeric complexes are shifted with respect to the spectrum of the bare chromophore, as a result of the different strength of the intermolecular interactions in the ground and excited states.

By fixing the UV ionization laser to one of the cluster-specific transitions in its R2PI spectrum, the vibrational spectra in the OH-stretching region of the neutral precursors have been recorded by IR-R2PI double-resonance spectroscopy. The IR and UV lasers are counterpropagating and spatially superimposed, the IR laser pump pulse precedes the UV laser by about 100 ns. In case a cluster absorbs photons with energies of a high-frequency vibrational mode, it predissociates very fast by

intramolecular vibrational redistribution (IVR) resulting in a depopulation and an R2PI ion signal depletion. The ion-dip spectra represent the vibrational spectrum of the neutral precursor cluster in the electronic ground state. This methodology also allows us to distinguish bands from isomeric structures, and spectral features deriving from the fragmentation of larger complexes.[20]

The IR laser light is generated using a recently homemade, injection-seeded optical parametric oscillator (OPO), which has been built according to a design developed at the University of Frankfurt.[21] It utilizes a Nd:YAG pump laser, a tunable dye laser and $LiNbO_3$ crystals. Typical energies are about 2 mJ per pulse. The wavelength may be tuned in the range 2.5–4.0 μm with a bandwidth of 0.8 cm^{-1}, except for a dip in between 2.84 and 2.87 μm that is due to OH impurities in the $LiNbO_3$ crystals. The oFE_S, pFE_S, E_R, B_R and B_S samples were purchased from Apollo Scientific and Sigma Aldrich and were used without further purification.

2.2 Theoretical section

The computational methodology adopted for the study of the bimolecular adducts relevant for this work is based on a two-level approach. At the first level we have characterized the conformational landscape of the potential energy surface (PES) of the here studied molecular systems by means of classical molecular dynamics based on the MM3 force field at a temperature of 800 K with constraints to overcome dissociation (cumulative time of 0.1 ns, dump time of 1 ps). 100 snapshots are then optimized with a convergence of 10^{-6} kcal (mol Å)$^{-1}$ RMS gradient per atom. The optimized structures are then classified according to their topology. At this level of calculations the Tinker program has been used.[22] Lowest energy structures (these procedure selects a total of 46 bimolecular adducts) for each diastereomer (relative energy lower than 2 kcal mol^{-1}) have been re-optimized at the second level approach: density functional theory corrected by dispersion interactions as developed by Grimme.[23] The *ab initio* calculations have been performed with the 6-31++G** basis set. The frequency analysis has been based on normal mode harmonic approximation, and a scaling factor of 0.9613 has been used. Test calculations on a subset of the 46 structures have been performed at the MP2/6-31++g** level of theory (with geometry optimization and frequency calculations with the smaller basis set 6-31g*, a frequency scaling factor of 0.943). All the above *ab initio* calculations have been executed with Gaussian09,[24] NWCHEM,[25] and GAMESS-US[26] program packages.

The intermolecular energies of the 46 adducts, in their D-DFT optimized geometry, have been classified in a semi-quantitative form with respect to the nature of the interaction: OH···π, CH···π, OH···F, CH···F, hydrogen bond. An energy component breakdown analysis has been carried out by means of a classical MM3 force field in which the CH···F interaction has been provided as a H-bond term with an equilibrium distance of 2.92 Å and a well depth of 0.19 kcal mol^{-1} to reproduce high level quantum calculations of benzene–methane interaction,[27] whereas the CH···π interaction has been simulated as a H-bond term with an equilibrium distance of 3.14 Å and a well depth of 0.23 kcal mol^{-1} to reproduce high level quantum calculations of fluorobenzene–methane interaction.[28]

3. Experimental results on the homo and heterochiral complexes of oFE_S with butan-2-ol

3.1 Mass selective electronic spectroscopy: R2PI excitation spectra

Fig. 2a–d report the R2PI excitation spectra obtained by supersonic expansion of a mixture of oFE_S with B_R (a,b) or B_S (c,d) pure enantiomer vapors. The spectra were acquired by monitoring the chromophore (m/z = 140) and the complex parent ion signals (m/z = 214) in the same wavelength scans. Owing to the large ionic dissociation of the complexes by R2PI ionization, the spectra of the bare chromophore acquired under the same conditions (Fig. 2a and c) present additional bands ($0_0^0{}_{hetero}$, α, β in Fig. 2a and α′ in Fig. 2c) which are due to the hydrogen bond dissociation of the ionic diastereomeric complexes in the $[oFE_S]^+$ mass channel.

The spectrum of the heterochiral complex (Fig. 2b) is characterized by a $0_0^0{}_{hetero}$ band origin at 37 513 cm^{-1}, red shifted relative to the $S_1 \leftarrow S_0$ origin of the isolated oFE_S molecule by $\Delta\nu = -74$ cm^{-1}. This band is followed by a 20 cm^{-1} spaced low-frequency progression (bands α and β). Further to the blue several bands of appreciable intensity are present at +92 and +108 cm^{-1} (bands γ and δ) from the 0_0^0 origin of the complex.

Differently from the heterochiral adduct, the R2PI excitation spectrum of the homochiral diastereoisomer, Fig. 2d, is blue-shifted ($\Delta\nu$ = +4 cm^{-1}) with respect to the 0_0^0 transition of the bare chromophore. This indicates a larger gap between the excited and the ground state energy of the cluster relative to that of the bare chromophore. This spectrum is characterized by three strong bands: the $0_0^0{}_{homo}$ transition at 37 591 cm^{-1} and a vibrational progression spaced about 19 cm^1 apart (bands α′ and β′) followed further to the blue by some bands of weaker intensity.

3.2 Vibrational spectroscopy: IR-R2PI spectroscopy

The vibrational spectra of the neutral diastereomers in the OH-stretching region have been recorded by IR-R2PI double-resonance spectroscopy. The spectra have been registered by scanning the wavelength of the IR laser with the UV-probe laser being fixed in turn to all the cluster-specific transitions in their R2PI spectrum.

Fig. 3 reports the IR-R2PI spectra of the homo and hetero complexes recorded in the 3500–3800 cm^{-1} range. The spectrum in Fig. 3a is recorded using the UV-probe set on the $S_1 \leftarrow S_0$ origin of the homochiral complex (37 591 cm^{-1}, band $0_0^0{}_{homo}$ in Fig. 2d) while the spectrum in Fig. 3b has been taken using the UV-probe set on the $S_1 \leftarrow S_0$ origin of the heterochiral complex (37 513 cm^{-1}, band $0_0^0{}_{hetero}$ in Fig. 2a and b). Both spectra show only one sharp absorption at 3636 cm^{-1} for the homochiral complex and at 3616 cm^{-1} for the heterochiral complex with comparable intensity depletion.

The UV-probe laser was also set on the other bands in the UV spectra to verify whether other conformers were present in

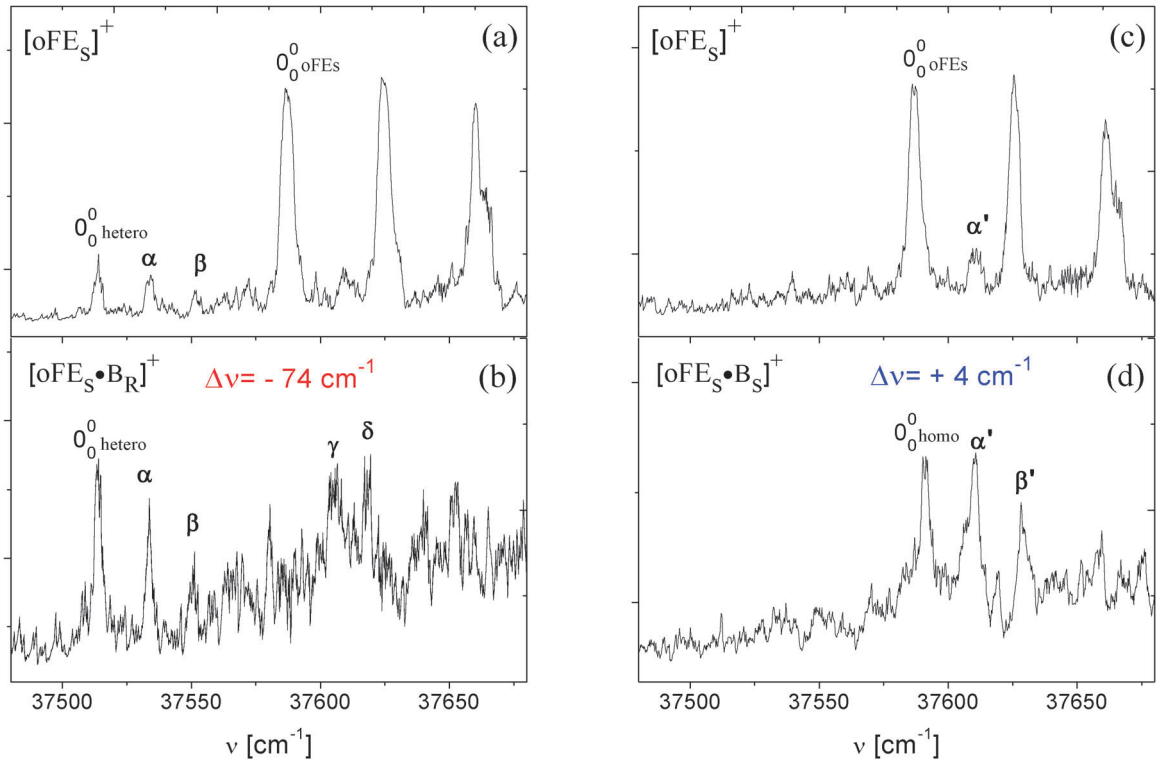

Fig. 2 R2PI spectra acquired by monitoring the bare molecular ion $[oFE_S]^+$ at m/z = 140 and the $[oFE_S{\cdot}B]^+$ cluster signal at m/z = 214: (a) $[oFE_S]^+$ in the presence of B_R (b) heterochiral $[oFE_S{\cdot}B_R]^+$ (c) $[oFE_S]^+$ in the presence of B_S (d) homochiral $[oFE_S{\cdot}B_S]^+$.

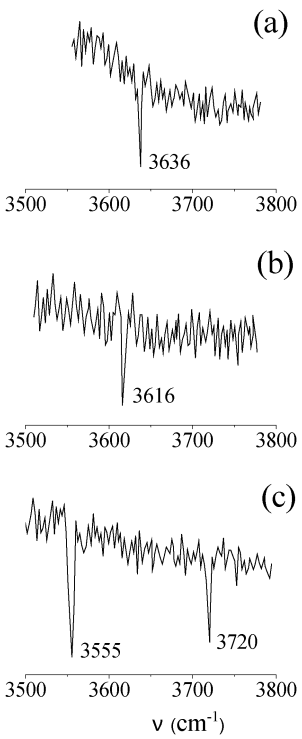

Fig. 3 IR-R2PI spectra of the clusters of oFE_S with butan-2-ol: (a) homochiral, probe set at 37 591 cm^{-1} (band $0_0^0{}_{homo}$ in Fig. 2d). The spectra acquired with the probe set on bands α′ and β′ are comparable (b) heterochiral, probe set at 37 513 cm^{-1} (band $0_0^0{}_{hetero}$ in Fig. 2b). The spectra acquired with the probe set on bands α and β are comparable (c) heterochiral, probe set at 37 606 cm^{-1} (band γ in Fig. 2b).

the beam. The IR depletion spectra measured using the UV probe set on bands α′ and β′ of the homochiral adduct, not shown here, were similar to that of Fig. 3a, with a dip at 3636 cm^{-1}. Likewise, the IR depletion spectra measured using the UV probe set on bands α and β in the spectra of the heterochiral cluster were similar to the spectrum shown in Fig. 3b, with a dip at 3616 cm^{-1}. Therefore it can be affirmed that bands $0_0^0{}_{homo}$, α′ and β′ in Fig. 2d belong to the same homo conformer and bands $0_0^0{}_{hetero}$, α and β in Fig. 2b to the same hetero conformer. Differently, when the UV probe laser was set at the frequencies of bands γ and δ in Fig. 2b, the IR depletion spectra showed two absorptions bands at 3555 cm^{-1} and 3720 cm^{-1} (Fig. 3c). These values of the infrared frequencies are consistent with those attributable to the OH stretching of a hydrogen bonded water molecule[20a,29] and presumably they pertain to a hydrated hetero complex which, upon ionization, quantitatively fragments in the $[FE_S{\cdot}B_R]^+$ mass channel. Bands γ and δ will be disregarded in what follows and will be the subject of a future publication.

In summary, only one conformer was observed in the supersonic beam for both homo and hetero complexes, although we cannot exclude that some of the other low intensity bands in the spectra of Fig. 2 pertain to other conformers present in a minor amount, but these bands are not well resolved and too weak to be probed.

3.3 Mass spectrometry: $[oFE_SB_{S/R}]^+$ dissociation ratios in the R2PI process

The dissociation of the ionic complexes induced by 1-color R2PI is due to the fact that the S_1 excited states of the

complexes are higher in energy than one-half of their ionization energy. By the absorption of two photons, the ion is produced with a non-negligible excess energy, which results in vibrational excitation of the ionized species. This excitation causes the cluster ion to dissociate into its original components. The dissociation ratio $I_{[oFE_S]^+}/I_{[oFE_S]^+} + I_{[oFE_SB_{S/R}]^+}$ can be estimated from the intensity of the diastereomeric parent ion $I_{[oFE_SB_{S/R}]^+}$ and that of the dissociation product $I_{[oFE_S]^+}$ in the mass spectra recorded at specific R2PI transitions. In order to compare the extent of homo and hetero ion dissociation in the *ortho* substituted complex, we chose two absorption bands in the corresponding R2PI spectra where the overall energy ($E_{2h\nu}$) imparted to the neutral homo and hetero complexes is similar and which are not superimposed to absorption bands of the bare oFE_S molecule. The bands marked β in Fig. 2a and b and α′ in Fig. 2c and d satisfy these conditions.

The dissociation ratios in several experimental runs are highly reproducible and their values, averaged on several mass spectra, are 51% for the homo and 62% for the hetero complex at 75 220 cm^{-1} (band α′ and at 75 106 cm^{-1} band β) of total ionization energy respectively.

The dissociation ratio is related to the amount of excess vibrational energy within the ion complex and, under the same conditions,[30] should be higher for the diastereomer with a lower appearance threshold for the molecular $[oFE_S]^+$ ion from the ionized complex.

From the above data, we can observe that the dissociation ratio is slightly higher for the heterochiral complex, despite the ionization energy imparted in the 1cR2PI process is even lower. Therefore, we can presume that the neutral homochiral complex is more stable than the neutral heterochiral one.

This experimental finding is in line with previous experimental results in analogous systems *i.e.* 4-fluorophenyl-ethanol/butan-2-ol,[18] 1-phenyl-1-ethanol/butan-2-ol,[15,16] 1-phenyl-1-propanol/butan-2-ol,[31] where it was found that homochiral complexes were more stable than the heterochiral ones.

Moreover, we can compare the hetero/homo ratio in the fragmentation efficiency in the one-colour two-photon ionization of the complexes under analogous experimental conditions, assuming that this ratio is an indication of the relative stability of the specific neutral homo *versus* hetero complexes. The ratio is much higher for the *para* substituted complexes (88%/51% = 1.73)[18] with respect to the non-fluorinated (58%/50% = 1.16)[32] and *ortho* substituted (62%/51% = 1.22) adducts. This is an indication that the binding energy difference between the diastereomers is higher in the *para* substituted complexes with respect to the non-fluorinated and *ortho* substituted ones. The binding energy difference ΔD_0 has been measured in two color R2PI experiments by our group[16] and by Mons *et al.*[14] for the non-fluorinated complexes and resulted to be ΔD_0 ($E_R{\cdot}B_{R/S}$) = 0.7–1.0 kcal mol^{-1} while for the *para* substituted complexes only a lower limit has been measured: ΔD_0 ($pFE_S{\cdot}B_{R/S}$) > 0.6 kcal mol^{-1}.[18]

4. Theoretical results on homo and heterochiral complexes oFE_S, pFE_S and E_R with butan-2-ol

The most stable calculated conformational structures of the isolated chromophores oFE_S, pFE_S and E_R, which were also identified experimentally in the supersonic beam expansion, have already been reported.[33,34] They are remarkably similar: they are characterized by an intramolecular OH···π bond and a weak attractive $C_{ortho}H\cdots O$ interaction. In oFE_S there is also a weak $C_\alpha H\cdots F$ interaction.

Fig. 4a–c show the D-B3LYP calculated structures of the most stable ground-state homo and heterochiral complexes of oFE_S, pFE_S and E_R with *R* and *S* butan-2-ol (Bu). D-B3LYP structures of pFE_S with *R* and *S* butan-2-ol have already been reported,[18] but are shown here for comparison. A complete description of all calculated complexes is given in the ESI.†

In general, covalently bound fluorine hardly ever acts as an acceptor for available Brönsted acidic sites in the presence of competing heteroatom acceptors. Therefore the most stable structures of these complexes are all characterized by an OH···O hydrogen bond. The butan-2-ol molecule acts as a proton acceptor from the hydroxyl group of the chromophore ($O^{ch}H$), therefore replacing the intramolecular $O^{ch}H\cdots\pi$ interaction by a stronger intermolecular $O^{ch}H\cdots O^{bu}$ hydrogen bond (O^{bu} is the oxygen atom of butan-2-ol). The relative stability of these structures arises from an interplay of several

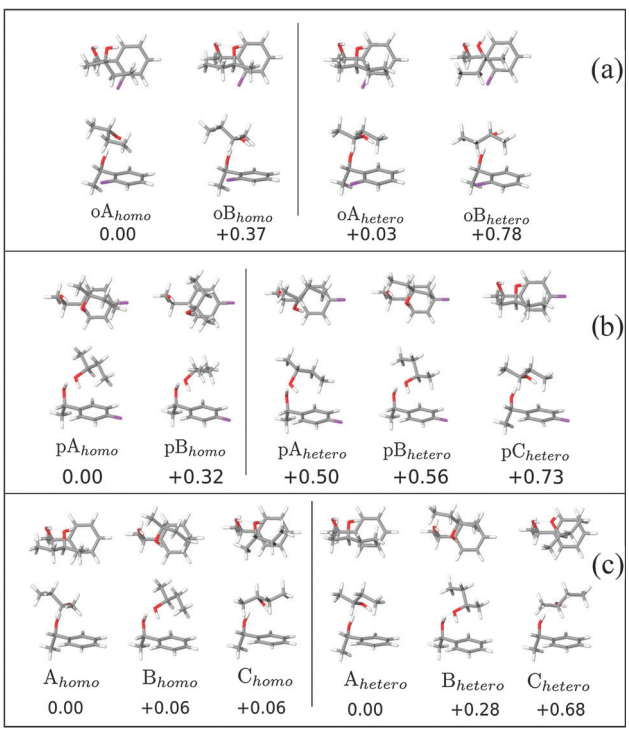

Fig. 4 D-B3LYP/6-31++G** structures and relative energies (kcal mol^{-1}) of some of the most stable homochiral and heterochiral conformers of the complexes of oFE_S, pFE_S and E_R with butan-2-ol. (a) *ortho* Fluorine substituted complexes, energies relative to the most stable oA_{homo} adduct. (b) *para* Fluorine substituted complexes, energies relative to the most stable pA_{homo} adduct, (c) non-fluorinated complexes, energies relative to the A_{homo} adduct.

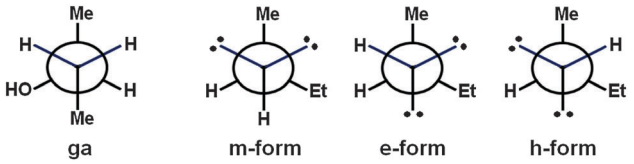

Fig. 5 Most stable C^2–C^3 conformation (ga) and the three C^2–O conformations of butan-2-ol.

contributions: the strength of the hydrogen bond which is the main electrostatic interaction and other intermolecular $O^{bu}H\cdots\pi$, $C^{bu}H\cdots\pi$, $C^{bu}H\cdots F$ or $O^{bu}H\cdots F$ contacts compete with each other for the stability of the hydrogen-bonded adducts.

In principle, several conformations of the chromophore and of butan-2-ol corresponding to rotations around C–C or C–O bonds are possible. The chromophores in the most stable complexes are characterized by the same conformation of the isolated molecule. For what concerns butan-2-ol, all the lowest energy calculated structures have a C^2–C^3 bond conformation which is the most stable and has been denoted "ga" by Lahmani *et al.*[35] (Fig. 5), where the first letter denotes the relation of the hydroxyl group and the methyl group and the second letter the relation of the two methyl groups. Several low energy structures with different C^2–O conformations of the butan-2-ol moiety have been found. As described by King and Howard,[36] these are denoted by a prefix that can be either "h," "m," or "e" depending on whether the hydroxyl hydrogen is located anti to a hydrogen, methyl, or ethyl group, as illustrated in Fig. 5.

Table 1 reports the geometrical parameters of the most stable D-B3LYP calculated structures and the specific conformation of butan-2-ol in the complex, while Table 2 reports the experimental and theoretical values of the OH stretching frequencies of butan-2-ol ($\nu O^{bu}H$) and of the C_1–C_α torsion (ν_1) in the complex, together with the energies of the calculated structures.

For a better evaluation of the relative energy of the complexes, as a test, some pertinent geometries with small relative energy were also optimized at the MP2/6-31g* theoretical level. This did not lead to a substantial change in the geometrical parameters, whereas frequency calculation at the MP2/6-31g* level of theory resulted in values for the OH stretching frequencies which were in great disagreement with the experimental ones. These values are reported in brackets in Table 2.

As shown in Table 1, some of the *ortho* fluorine substituted complexes are characterized by a CH···F distance, which is lower than the sum of the van der Waals radii of H and F, while CH···F interactions in the *para*-complexes are present but weaker. At variance with other systems[20a,37–38] we have found the presence of OH···F interactions only in complexes much higher in energy.

5. Assignment of the observed complexes

The assignment of the observed complexes to the calculated structures has been accomplished on the basis of (1) the comparison between calculated and observed vibrational

Table 1 Geometrical parameters of the most stable D-B3LYP/6-31++g** calculated structures with indication of the butan-2-ol conformation

Complex structure (conformation of butan-2-ol)	Interaction	$R(\theta)^a$ (Å(deg))
OA_{hetero} (m-ga)	$C^4H\cdots\pi$	3.2 (24)
	$C^4H\cdots F$	3.67
	$C^2H\cdots\pi$	3.33 (44)
	$C^2H\cdots F$	2.81
	$OH\cdots\pi$	2.98 (33)
	H-bond	1.87 (158)
oB_{hetero} (e-ga)	$C^1H\cdots\pi$	2.54 (2)
	$C^3H\cdots F$	2.61
	$OH\cdots\pi$	4.32 (39)
	H-bond	1.82 (173)
oA_{homo} (m-ga)	$C^4H\cdots\pi$	2.58 (3)
	$C^3H\cdots\pi$	3.48 (46)
	$C^3H\cdots F$	2.54
	$OH\cdots\pi$	3.28 (36)
	H-bond	1.82 (164)
oB_{homo} (e-ga)	$C^1H\cdots\pi$	3.23 (27)
	$C^1H\cdots F$	4.13
	$C^2H\cdots\pi$	3.33 (45)
	$C^2H\cdots F$	2.66
	$OH\cdots\pi$	2.83 (30)
	H-bond	1.91 (156)
pA_{homo} (m-ga)	$C^4H\cdots\pi$	3.19 (29)
	$C^4H\cdots F$	3.00
	$C^2H\cdots\pi$	3.23 (33)
	$OH\cdots\pi$	2.83 (28)
	H-bond	1.87 (160)
pB_{homo} (h-ga)	$C^3H\cdots\pi$	2.98 (19)
	$C^3H\cdots F$	3.71
	$C^1H\cdots F$	4.71
	$C^1H\cdots\pi$	4.29 (22)
	$OH\cdots\pi$	2.80 (32)
	H-bond	1.9 (159)
pA_{hetero} (m-ga)	$C^4H\cdots\pi$	2.56 (24)
	$OH\cdots\pi$	3.15 (33)
	H-bond	1.83 (161)
pB_{hetero} (e-ga)	$C^1H\cdots\pi$	3.07 (24)
	$OH\cdots\pi$	2.77 (33)
	H-bond	1.91 (161)
pC_{hetero} (m-ga)	$C^4H\cdots\pi$	3.11 (24)
	$C^4H\cdots F$	3.70
	$C^2H\cdots\pi$	3.31 (42)
	$OH\cdots\pi$	2.97 (33)
	H-bond	1.86 (161)
A_{hetero} (m-ga)	$C^4H\cdots\pi$	3.08 (22)
	$C^4H\cdots\pi$	3.72 (13)
	$C^2H\cdots\pi$	3.28 (41)
	$OH\cdots\pi$	2.97 (33)
	H-bond	1.86 (161)
B_{hetero} (e-ga)	$C^1H\cdots\pi$	3.09 (19)
	$C^2H\cdots\pi$	3.34 (39)
	$OH\cdots\pi$	2.74 (28)
	H-bond	1.91 (158)
C_{hetero} (m-ga)	$C^2H\cdots\pi$	2.45 (9)
	$C^4H\cdots\pi$	3.86 (31)
	$C^1H\cdots\pi$	3.91 (47)
	$OH\cdots\pi$	3.47 (40)
	H-bond	1.87 (165)

Table 1 (*continued*)

Complex structure (conformation of butan-2-ol)	Interaction	$R(\theta)^a$ (Å(deg))
A_{homo} (e-ga)	$C^1H\cdots\pi$	3.16 (20)
	$C^2H\cdots\pi$	3.42 (46)
	$OH\cdots\pi$	2.78 (29)
	H-bond	1.90 (159)
B_{homo} (m-ga)	$C^4H\cdots\pi$	3.12 (26)
	$C^2H\cdots\pi$	3.21 (32)
	$OH\cdots\pi$	2.90 (31)
	H-bond	1.87 (160)

[a] See Scheme 1 for details. In the case of the H-bond θ is referred to the O–H–O angle.

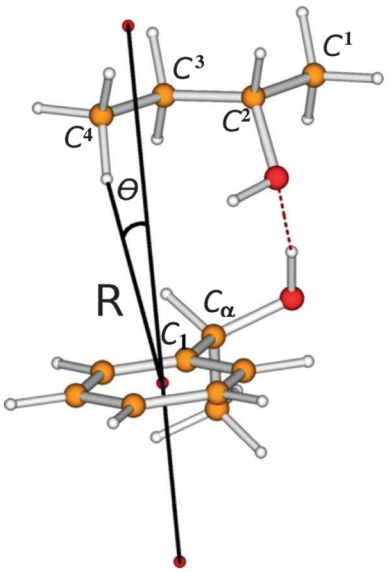

Scheme 1 Atom-numbering scheme in butan-2-ol and *R* and θ definitions.

frequencies, (2) the analysis of the specific interactions contributing to the shift of the electronic transition, (3) the relative energy of the complexes.

The last two points deserve more comments. The different values of the electronic spectral shifts reflect the combined effects of electrostatic and dispersive interactions on the energies of the S_0 and S_1 states of the diastereomeric adducts. Specifically intermolecular forces such as $CH\cdots\pi$ and $OH\cdots\pi$ interactions are relevant for these complexes.[39] $CH\cdots\pi$ interactions are stronger in the S_1 state because of enhanced dispersion forces due to the higher polarizability of the aromatic molecule in the excited state, and contribute to a red-shift of the $\pi^* \leftarrow \pi$ transition. On the other hand $OH\cdots\pi$ interactions are known to contribute to a decrease in the binding energy in the excited state of chromophores with only one benzenoid ring, and therefore contribute to the blue of the electronic transition.[40] The specific impact of $CH\cdots F$ interactions on the shift of the $\pi^* \leftarrow \pi$ electronic transition is somewhat less clear, depending on different effects such as geometrical deformation, the position of the fluorine atom

Table 2 D-B3LYP6-31++g** and single point MP2/6-31++g** energies of $oFE_S{\cdot}B_{S/R}$, $pFE_S{\cdot}B_{S/R}$, and $E_R{\cdot}B_{S/R}$, relative to the corresponding most stable homo complex and experimental ν_1 frequencies of the S_1 excited state and $\nu O^{bu}H$ frequencies of the S_0 ground state of the complexes compared with the D-B3LYP/6-31++g** and MP2/6-31g* calculated vibrational frequencies for the S_0 ground state

		Energy relative to the most stable homo conformer (kcal mol^{-1})		ν_1 (cm^{-1})		$\nu O^{bu}H$ (cm^{-1})	
Complex	Conformer structure	D-DFT[a]	MP2 sp	Exp	D-DFT (MP2)	Exp	D-DFT (MP2)
$oFE_S{\cdot}B_R$	oA_{hetero}	0.03	0.11	20	19.9	3616	3643
	oB_{hetero}	0.78	0.44		30.1		3684
	oC_{hetero}	0.80	0.79		30.5		3653
$oFE_S{\cdot}B_S$	oA_{homo}	0.00	0.03	19	40 (29)	3636	3661 (3533)
	oB_{homo}	0.37	0.00		25 (29)		3635 (3489)
$pFE_S{\cdot}B_R$	pA_{hetero}	0.50	0.82	19	27	3610	3672
	pB_{hetero}	0.56	0.75		33		3659
	pC_{hetero}	0.73	1.30		23		3610
$pFE_S{\cdot}B_S$	pA_{homo}	0.00	0.00	17	23	3637	3635
	pB_{homo}	0.32	0.52		35		3602
$E_R{\cdot}B_S$	A_{hetero}	0.00	0.05	17	29.0		3634
	B_{hetero}	0.28	0.00		28.5		3627
	C_{hetero}	0.68	0.07		15.5		3673
	D_{hetero}	0.68	0.38		21.7		3602
	E_{hetero}	0.68	0.71		11.2		3638
$E_R{\cdot}B_R$	A_{homo}	0.00	0.02	17	28.2		3624
	B_{homo}	0.06	0.00		23.4		3634
	C_{homo}	0.06	0.48		25.2		3652
	D_{homo}	0.54	0.31		18.1		3648

[a] A fair estimate of the accuracy of D-B3LYP/6-31G** energy calculation is of the order of 0.5 kcal mol^{-1}.

and its dual nature in the electron donating/withdrawing character.

It is difficult to predict the relative abundance of the complexes, which are formed and stabilized during the free jet expansion, only on the basis of the most stable calculated conformations. In fact the formation of the complexes in the collision zone is affected by complex kinetic and thermodynamic factors.[41] The collisional relaxation may partly drain the population into the most stable conformational structures if the interconversion[42] barriers between conformers are sufficiently low. It is also possible that isomers that are calculated to be the most stable ones are not observed experimentally.[41c] Moreover, calculations often predict small energy differences between the isomers, so that we cannot be always confident of the energy order. We have taken into account for the assignment all the structures which, at the D-B3LYP/6-31++G** level of theory, have a relative energy of below 1.2 kcal mol^{-1}.

5.1 Assignment of the *ortho* fluorine substituted complexes

The bands at 3636 and 3616 cm^{-1} in the IR-R2PI spectra (Fig. 3a and b) correspond to the OH stretch mode of butan-2-ol in these clusters (νO^bH). IR-R2PI spectroscopy indicates that only one conformer of each homo and hetero complexes was present under our experimental conditions. On the basis of these data and as explained below, the structures oB_{homo} and oA_{hetero}, calculated among the more stable complexes, give the best overall agreement with the experimental data. In fact, D-B3LYP calculations predict the νO^bH stretching frequency for conformer oB_{homo} at 3635 cm^{-1}, in full agreement with the IR-R2PI measured value (Table 2). The low-frequency progression spaced 19 cm^{-1} (Fig. 2d, Table 2) is attributable to the C_1–C_α torsion calculated at 25.0 cm^{-1} for the ground S_0 state of conformer oB_{homo}. For the heterochiral complex, the best agreement between the calculated value of the νO^bH stretching frequency and the measured one is for oA_{hetero} (Table 2). The low-frequency progression spaced 20 cm^{-1} (Fig. 2b) is attributable to the C_1–C_α torsion calculated at 19.0 cm^{-1} for the ground S_0 state of conformer oA_{hetero}.

The assignment is supported by the analysis of the geometric parameters associated with the intermolecular forces at play in the S_1 and S_0 electronic levels.

The small value of the blue shift of the electronic transition of the homo cluster and the red shift of the hetero cluster can be rationalized in terms of the relative strength of the intermolecular forces: in oB_{homo} the OH$\cdots\pi$ interaction established between the hydroxyl group of B_R and the aromatic ring of oFE_S is stronger ($O^{bu}H\cdots\pi$ distances 2.83 Å in oB_{homo} and 2.98 Å in oA_{hetero}) and CH$\cdots\pi$ interactions are weaker in oB_{homo} with respect to oA_{hetero}. Therefore it is expected that oA_{hetero} is rather red-shifted with respect to oB_{homo}, in agreement with the experimental finding.

5.2 Assignment of the *para* fluorine substituted complexes

In our previous work[18] we assigned the measured spectra of *para* fluorine substituted complexes on the basis of the comparison between calculated and observed vibrational frequencies and binding energies. The homochiral and heterochiral complexes were attributed to the structures pA_{homo} and pC_{hetero}. In both structures the hydroxyl hydrogen atom of butan-2-ol is pointing towards the aromatic ring and OH$\cdots\pi$ interactions are quite strong, as well as CH$\cdots\pi$ interactions.

5.3 Assignment of the non-fluorinated complexes

Only one conformer was observed in the supersonic beam for the homo complex while the hetero system possibly exhibits two isomers. The less abundant hetero complex has been observed by Le Barbu *et al.*[15] by UV-UV depletion spectroscopy and has a population of less than 20%. The homo and the most abundant conformer of the hetero cluster have been assigned by Zehnacker *et al.*[43] to complexes in which the C^2–C^3 conformation of butan-2-ol is ga. This is in agreement with our results which predict that these structures are the most stable ones. Both the homo and hetero complexes display a red shift of the electronic transition relative to the electronic origin of the isolated chromophore. The red shift of the most abundant heterochiral complex ($\Delta\nu = -131$ cm^{-1}) exceeds that of the homochiral one ($\Delta\nu = -119$ cm^{-1}) by $\Delta\Delta\nu = 12$ cm^{-1}.

The observed homo complex can be assigned to B_{homo} while the most abundant hetero complex can be assigned either to C_{hetero} or to A_{hetero}. The OH$\cdots\pi$ forces are stronger in B_{homo} (OH$\cdots\pi$ distance 2.90 Å) with respect to C_{hetero} (OH$\cdots\pi$ distance 3.47 Å) or A_{hetero} (OH$\cdots\pi$ distance 2.97 Å). It is therefore expected that A_{hetero} or C_{hetero} is rather red-shifted with respect to B_{homo} and indeed this conforms to the experimental data. The assignment of the heterochiral complex to the C_{hetero} calculated structure is supported[44] by a better agreement, with respect to A_{hetero}, between the measured values of the low-frequency progressions and the C_1–C_α torsion calculated for the ground S_0 state of the complexes (Table 2). However a deeper inspection of the geometrical parameters indicates that C_{hetero} is quite different from the other assigned structures, in fact has the hydroxyl hydrogen atom pointing outside the aromatic ring and is characterized by a particularly short $C^2H\cdots\pi$ distance (2.45 A). Since the spectroscopic behavior of the most abundant non-fluorinated hetero complex is much similar to the other hetero complexes (pC_{hetero}[18] and oA_{hetero}), we are more inclined to assign it to the A_{hetero} structure.

6. Comparison between the different systems and the role of the fluorine substitution

The comparison between all the structures assigned on the basis D-B3LYP/6-31++G** calculations reveals some interesting aspects, which enable us to figure out a picture of the chiral discrimination process in these systems.

It is worth pointing out that the structural assignment was accomplished without taking the specific conformation of the butan-2-ol moiety in the complex into account. Nevertheless, an inspection of the assigned structures reveals that the conformation of butan-2-ol in the clusters is always the m-ga one, except

for the homo *ortho* substituted complex (oB_{homo}) where the conformation of butan-2-ol is e-ga. The e-ga and m-ga conformations have been identified by microwave Fourier transform spectroscopy of butan-2-ol[36,45] in supersonic beam expansion and have been predicted to be the most stable conformations at the MP2/6-311++G** level of theory with e-ga more stable than m-ga by 98 cm^{-1} and a barrier between them of 308 cm^{-1}. As mentioned previously, the aromatic chromophore has an anti conformation in all the assigned complexes. Furthermore, in all the complexes the ethyl group of butan-2-ol is bent over the aromatic ring, except for oB_{homo}, in which the methyl group of B_R interacts with the aromatic ring.

Another interesting aspect that emerged after the assignment is the similarity of the binding motif within the homo or the hetero class of compounds. Specifically, within the homo class of compounds, pA_{homo} and B_{homo} assigned structures are remarkably similar (see Fig. 4b and c), while within the hetero class of compounds oA_{hetero}, pC_{hetero} and A_{hetero} (Fig. 4) structures resemble each other.

The structural arrangement of the two interacting molecules can be described as follows: the OH group of butan-2-ol inserts itself into the $O^{ch}H\cdots\pi$ linkage of the chromophore, forming an $O^{ch}H\cdots O^{bu}$ hydrogen bond and an $O^{bu}H\cdots\pi$ interaction with the aromatic ring (see Fig. 6). The hydrogen atom attached to the C^2 chiral center of butan-2-ol also points towards the aromatic ring, so that $C^2H\cdots\pi$ interactions are established. Other $C^2H\cdots\pi$ interactions can be established either by facing the ethyl or the methyl group of butan-2-ol towards the aromatic ring, yet these interactions are stronger if the ethyl points towards the aromatic ring. Except for oB_{homo}, which will be discussed further in this paper, the preferred arrangement of these complexes involves an interaction of the ethyl group with the aromatic ring. However, the different chirality of the two stereoisomers of butan-2-ol involves that, in the complex, the hydrogen atom attached to the C_α chiral center of the aromatic molecule and the hydrogen atom attached to the C^2 chiral center of butan-2-ol are facing each other in the hetero complexes, while they point to opposite directions in the homo complexes (Fig. 6). Consequently $C_\alpha H\cdots HC^2$ repulsive interactions in the hetero complexes are somewhat more relevant, decreasing the overall $CH\cdots\pi$ and $OH\cdots\pi$ interactions with the aromatic ring. Indeed the ethyl group of butan-2-ol is more overlapping on the aromatic ring in the homo complexes with respect to the hetero adducts (compare pA_{homo} and pC_{hetero} or B_{homo} and A_{hetero} in Fig. 4b and c). This is in agreement with the experimental findings that the homo complexes are more stable than the hetero complexes.

The comparison between the *para* fluoro and non-fluorinated complexes reveals that the presence of the fluorine atom in the *para* position of the aromatic ring does not affect the overall geometry of the complex, though in the *para* homo complex a contraction of the vdW complex with a shortening of the $OH\cdots\pi$ distance is recognizable, by comparison with the non-fluorinated homo complex (Table 1). Moreover, although the *para* F atom is situated far from the side chain, in the homo *para* fluorinated complex the ethyl group of butan-2-ol is able to establish very weak $C^4H\cdots F$ interactions ($H\cdots F$ distance 3.0 Å). The strengthening of the attractive interactions in the homo *para* complex can be tentatively attributed to the inductive and resonance effects of the fluorine atom on the aromatic ring, which modify the distribution of the π electron density. This probably leads to an extra stabilization of the homo *para* substituted complex with respect to the non-substituted homo adduct and could explain the fact that the experimental binding energy difference between the homo and hetero *para*-fluorine substituted complexes is evaluated to be higher than the binding energy difference in the non-fluorinated diastereomers. Furthermore, this trend is also predicted by the energy calculations at the D-B3LYP/6-31++G** and the single point MP2/6-31++G** level of theory (Table 2).

The fluorine atom in the *ortho* position brings on another asymmetry element in the aromatic molecule. In fact, the *ortho* substituted bare molecule is characterized by a weak $C_\alpha H\cdots F$ intramolecular interaction. In the complex formation, the fluorine atom is also available for the formation of an intermolecular $C^2H\cdots FC$ interaction. Considering a structural motif like the one described above for the *para* and non-fluorinated complexes (Fig. 6) the $C^2H\cdots FC$ interaction can be established only in the hetero *ortho* substituted complex. In the *ortho* homo adduct, the establishment of $C^2H\cdots F$ intermolecular interaction together with an $O^{bu}H\cdots\pi$ interaction is only possible if it is the methyl group that interacts with the aromatic ring and this implies that the C–O bond conformation of butan-2-ol must be different (e-ga). The UV spectroscopic behavior of the *ortho*-hetero complex is analogous to the other hetero structures (*para* and non-fluorinated), while only for the *ortho*-homo complex a blue shift of the electronic transition is observed. The different spectroscopic behavior of the homo *ortho* complex is in agreement with the fact that the conformation of butan-2-ol and/or the structural arrangement is different in this complex.[43]

The observation of the oB_{homo} complex acknowledges the role and the importance of $CH\cdots F$ interactions in molecular and chiral recognition processes. It also points out that chiral recognition does not result only from a simple approach of molecules. Apparently, during the formation of these complexes in supersonic expansion, in order to achieve the best compromise of intermolecular interactions, the butan-2-ol

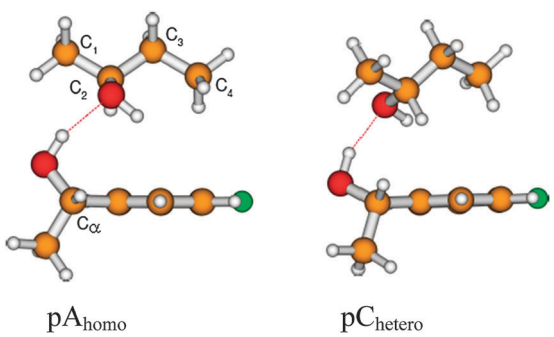

Fig. 6 Enlarged front view of the pA_{homo} and pC_{hetero} structures.

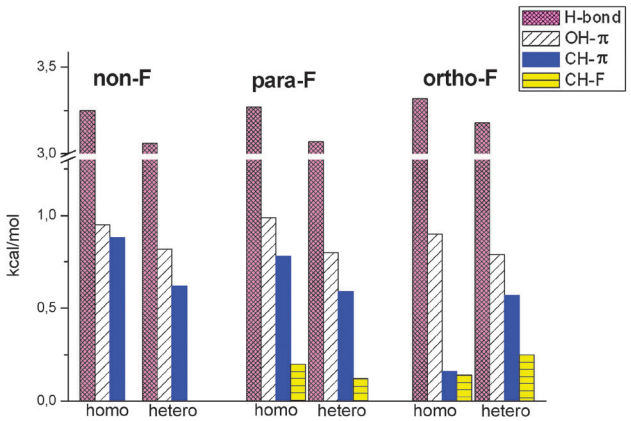

Fig. 7 Contribution of the OH···O, CH···π, OH···π and CH···F interactions to the total potential energy of the assigned structures, calculated with an MM3 force field at the D-B3LYP/6-31++G** geometries.

monomer switches to one conformation to another (either m-ga → e-ga or e-ga → m-ga). As a matter of fact, only one structure of the fluorine substituted complexes has been observed in the molecular beam, whereas in supersonic expansion of butan-2-ol several conformers have been identified.

Another purpose of the present work is to try to figure out the different contributions of the specific CH···π, OH···π, CH···F and hydrogen bond interactions to the total potential energy in order to find out if some contributions are primarily responsible for chiral discrimination in these systems.

Fig. 7 reports, in a histogram, the contribution of the specific intermolecular interactions for the assigned structures, which were calculated with a classical force field (MM3) at the D-DFT geometries. The complete table of values is reported in the ESI.† The outcome is in agreement with what has been previously inferred.[8a,43,44] The homo and heterochiral complexes of these molecules are endowed with very fine, subtle differences in the CH···π, OH···π and CH···F interactions and in the strength of the hydrogen bond. As shown in Fig. 7, this model evaluates that the homo *para* and non-fluorinated complexes are characterized by somewhat stronger CH···π, OH···π and CH···F (in *para* substituted complexes) interactions with respect to the hetero complexes. The intermolecular interactions in turn affect the strength of the hydrogen bond which is somewhat larger in the homo clusters with respect to the hetero complexes. These differences in the contributions make the total binding energy of the homo complexes higher compared to the binding energy of the hetero structures. It also results that in the homo *ortho*-fluorinated complex, CH···F interactions are established at the expense of CH···π interactions, the latter resulting stronger in the heterochiral adduct, which has the ethyl group pointing towards the aromatic ring.

7. Conclusions

The presented results and the above discussions provide the first detailed structural investigation that shows how the presence of fluorine on different positions of the aromatic ring is able to affect the chiral recognition process in isolated complexes.

Our combined experimental/theoretical investigation on clusters of structurally similar aromatic molecules with the same chiral partners enabled us to figure out a picture of the chiral discrimination process at the molecular level. The homo and heterochiral complexes between *ortho*, *para* and non-substituted 1-aryl-1-ethanol and butan-2-ol are characterized by the same binding motif and are endowed with very fine differences in CH···π, OH···π, CH···F as well as repulsive interactions, which in turn affect the strength of the hydrogen bond.

The substitution of a F atom in the *para* position does not influence the overall geometry of the complex whilst it affects the electron density in the π system and the strength of CH···π and OH···π interactions. This effect, together with the fact that in the homo complex a very weak $C^4H\cdots F$ interaction is established, results in a higher binding energy difference in the diastereomers of the *para* substituted compounds with respect to the homo diastereomers.

The role and the importance of CH···F intermolecular interactions are evident in the complexes with fluorine substitution in the *ortho* position. While the *ortho* hetero complex is structurally analogous to the hetero *para* and non-fluorinated structures, butan-2-ol in the *ortho* homo adduct adopts a different conformation in order to establish a CH···F intermolecular interaction.

Our results confirm at the molecular level that chiral recognition is a process that involves the conformational adjustments of the partners in order to achieve the best efficacy of non-covalent interactions.

References

1 (*a*) J. Bella, M. Eaton, B. Brodsky and H. M. Berman, *Science*, 1994, **266**, 75; (*b*) H. C. Chang, J. C. Jiang, C. M. Feng, Y. C. Yang, C. C. Su, P. J. Chang and S. H. Lin, *J. Chem. Phys.*, 2003, **118**, 1802; (*c*) S. Scheiner, T. Kar and J. Pattanayak, *J. Am. Chem. Soc.*, 2002, **124**, 13257; (*d*) P. Milko, J. Roithová and K. A. Schug, *Phys. Chem. Chem. Phys.*, 2013, **15**, 6113.

2 (*a*) D. Chopra and T. N. Guru Row, *CrystEngComm*, 2011, **13**, 2175; (*b*) K. L. Kirk, *J. Fluorine Chem.*, 2006, **127**, 1013; (*c*) C. Isanbor and D. O'Hagan, *J. Fluorine Chem.*, 2006, **127**, 303; (*d*) J. P. Bégué and D. Bonnet-Delpon, *J. Fluorine Chem.*, 2006, **127**, 992; (*e*) S. C. F. Kui, N. Zhu and M. C. W. Chan, *Angew. Chem., Int. Ed.*, 2003, **42**, 1628.

3 (*a*) J. P. Simons, *Mol. Phys.*, 2009, **107**, 2435; (*b*) T. S. Zwier, *J. Phys. Chem. A*, 2006, **110**, 4133; (*c*) B. Brutschy, *J. Phys. Chem.*, 1990, **94**, 8637–8647.

4 J. P. Shermann, *Spectroscopy and modelling of biomolecular building blocks*, Elsevier, Amsterdam, 2007.

5 A. R. Al Rabaa, E. Breheret, F. Lahmani and A. Zehnacker, *Chem. Phys. Lett.*, 1995, **237**, 480.

6 S. Piccirillo, C. Bosman, D. Toja, A. Giardini, M. Pierini, A. Troiani and M. Speranza, *Angew. Chem., Int. Ed. Engl.*, 1997, **36**, 1729.

7 N. Borho and M. Suhm, *Phys. Chem. Chem. Phys.*, 2002, **4**, 2721.

8 (*a*) A. K. King and B. Howard, *Chem. Phys. Lett.*, 2001, **348**, 343; (*b*) Z. Su, N. Borho and Y. Xu, *J. Am. Chem. Soc.*, 2006, **128**, 17126.
9 (*a*) D. Scuderi, K. Le Barbu-Debus and A. Zehnacker, *Phys. Chem. Chem. Phys.*, 2011, **13**, 17916; (*b*) A. Filippi, C. Fraschetti, S. Piccirillo, F. Rondino, B. Botta, I. D'Acquarica, A. Calcaterra and M. Speranza, *Chem.–Eur. J.*, 2012, **18**(27), 8320.
10 S. Portmann, A. Inauen, H. P. Luthi and S. J. Leutwyler, *Chem. Phys.*, 2000, **113**, 9577.
11 I. Alkorta, O. Picazo and J. Elguero, *Curr. Org. Chem.*, 2006, **10**, 695.
12 E. Kraka, M. Freindorf and D. Cremer, *Chirality*, 2013, **25**, 185.
13 A. Giardini Guidoni, S. Piccirillo, D. Scuderi, M. Satta, T. M. Di Palma and M. Speranza, *Phys. Chem. Chem. Phys.*, 2000, **2**, 4139.
14 M. Mons, F. Piuzzi, I. Dimicoli, A. Zehnacker and F. Lahmani, *Phys. Chem. Chem. Phys.*, 2000, **2**, 5065.
15 K. Le Barbu, A. Zehnacker, F. Lahmani, M. Mons, F. Piuzzi and I. Dimicoli, *Chirality*, 2001, **13**, 715.
16 A. Giardini Guidoni, S. Piccirillo, D. Scuderi, M. Satta, T. M. Di Palma, M. Speranza, A. Filippi and A. Paladini, *Chirality*, 2001, **13**, 727.
17 D. Scuderi, A. Paladini, M. Satta, D. Catone, A. Filippi, S. Piccirillo, A. Laganà, M. Speranza and A. Giardini Guidoni, *Int. J. Mass Spectrom.*, 2003, **223–224**, 159.
18 F. Rondino, A. Paladini, A. Ciavardini, A. Casavola, D. Catone, M. e. Satta, H. D. Barth, A. Giardini, M. Speranza and S. Piccirillo, *Phys. Chem. Chem. Phys.*, 2011, **13**, 818.
19 S. Piccirillo, M. Coreno, A. Giardini-Guidoni, G. Pizzela, M. Snels and R. Teghil, *J. Mol. Struct.*, 1993, **293**, 197.
20 (*a*) B. Brutschy, *Chem. Rev.*, 2000, **100**, 3891; (*b*) E. G. Robertson and J. P. Simons, *Phys. Chem. Chem. Phys.*, 2001, **3**, 1; (*c*) T. S. Zwier, *J. Phys. Chem. A*, 2006, **110**, 4133.
21 B. Reimann, K. Buchhold, H. D. Barth, B. Brutschy, P. Tarakeshwar and K. S. Kim, *J. Chem. Phys.*, 2002, **117**, 1.
22 P. Ren and J. W. Ponder, *J. Phys. Chem. B*, 2003, **107**, 5933.
23 S. Grimme, *J. Comput. Chem.*, 2006, **27**, 1787–1799.
24 M. J. Frisch, G. W. Trucks, H. B. Schlegel, G. E. Scuseria, M. A. Robb, J. R. Cheeseman, G. Scalmani, V. Barone, B. Mennucci, G. A. Petersson, H. Nakatsuji, M. Caricato, X. Li, H. P. Hratchian, A. F. Izmaylov, J. Bloino, G. Zheng, J. L. Sonnenberg, M. Hada, M. Ehara, K. Toyota, R. Fukuda, J. Hasegawa, M. Ishida, T. Nakajima, Y. Honda, O. Kitao, H. Nakai, T. Vreven, J. A. Montgomery, Jr., J. E. Peralta, F. Ogliaro, M. Bearpark, J. J. Heyd, E. Brothers, K. N. Kudin, V. N. Staroverov, R. Kobayashi, J. Normand, K. Raghavachari, A. Rendell, J. C. Burant, S. S. Iyengar, J. Tomasi, M. Cossi, N. Rega, J. M. Millam, M. Klene, J. E. Knox, J. B. Cross, V. Bakken, C. Adamo, J. Jaramillo, R. Gomperts, R. E. Stratmann, O. Yazyev, A. J. Austin, R. Cammi, C. Pomelli, J. W. Ochterski, R. L. Martin, K. Morokuma, V. G. Zakrzewski, G. A. Voth, P. Salvador, J. J. Dannenberg, S. Dapprich, A. D. Daniels, Ö. Farkas, J. B. Foresman, J. V. Ortiz, J. Cioslowski and D. J. Fox, *Gaussian 09, Revision A.1*, Gaussian, Inc., Wallingford, CT, 2009.
25 M. Valiev, E. J. Bylaska, N. Govind, K. Kowalski, T. P. Straatsma, H. J. J. van Dam, D. Wang, J. Nieplocha, E. Apra, T. L. Windus and W. A. de Jong, ''NWChem: a comprehensive and scalable open-source solution for large scale molecular simulations'', *Comput. Phys. Commun.*, 2010, **181**, 1477.
26 M. W. Schmidt, K. K. Baldridge, J. A. Boatz, S. T. Elbert, M. S. Gordon, J. H. Jensen, S. Koseki, N. Matsunaga, K. A. Nguyen, S. J. Su, T. L. Windus, M. Dupuis and J. A. Montgomery, *J. Comput. Chem.*, 1993, **14**, 1347.
27 A. L. Ringer, M. S. Figgs, M. O. Sinnokrot and C. D. Sherrill, *J. Phys. Chem. A*, 2006, **110**, 10822.
28 R. C. Dey, P. Seal and S. Chakrabarti, *J. Phys. Chem. A*, 2009, **113**, 10113.
29 K. Le Barbu, F. Lahmani, M. Mons, M. Broquier and A. Zehnacker, *Phys. Chem. Chem. Phys.*, 2001, **3**, 4684.
30 The total energy furnished in the process is almost equal for two diastereomers, the laser intensity is similar and the Franck–Condon window is located above the dissociation thresholds.
31 A. Latini, D. Toja, A. Giardini-Guidoni, S. Piccirillo and M. Speranza, *Angew. Chem., Int. Ed.*, 1999, 815–817.
32 Unpublished results: mass spectra from data reported in ref. 13.
33 (*a*) M. Speranza, F. Rondino, A. Giardini, A. Paladini, A. R. Hortal, S. Piccirillo and M. Satta, *ChemPhysChem*, 2009, **10**, 1859; (*b*) S. Tang and W. Caminati, *J. Mol. Spectrosc.*, 2010, **260**, 120.
34 K. Shin-ya, H. Sugeta, S. Shin, Y. Hamada, Y. Katsumoto and K. Ohno, *J. Phys. Chem. A*, 2007, **111**, 8598.
35 K. Le Barbu, V. Brenner, Ph. Millié, F. Lahmani and A. Zehnacker-Rentien, *J. Phys. Chem. A*, 1998, **102**, 128.
36 A. K. King and B. J. Howard, *J. Mol. Spectrosc.*, 2009, **257**, 205.
37 S. Chervenkov, P. Q. Wang, J. E. Braun, S. Georgiev, H. J. Neusser, C. K. Nandi and T. Chakraborty, *J. Chem. Phys.*, 2005, **122**, 244312.
38 A. Giardini, F. Rondino, G. Cattenacci, A. Paladini, S. Piccirillo, M. Satta and M. Speranza, *Chem. Phys. Lett.*, 2007, **435**, 230.
39 M. Satta, N. Sanna, A. Giardini and M. Speranza, *J. Chem. Phys.*, 2006, **125**, 094101.
40 A. J. Gotch, A. W. Garrett, D. L. Severance and T. S. Zwier, *Chem. Phys. Lett.*, 1991, **178**, 121.
41 (*a*) T. A. LeGreve, W. H. James III and T. S. Zwier, *J. Phys. Chem. A*, 2009, **113**, 399; (*b*) W. Y. Sohn, M. Kim, S. S. Kim, Y. D. Park and H. Kang, *Phys. Chem. Chem. Phys.*, 2011, **13**, 7037; (*c*) N. Seurre, J. Sepioł, K. Le Barbu-Debus, F. Lahmani and A. Zehnacker-Rentien, *Phys. Chem. Chem. Phys.*, 2004, **6**, 2867–2877.
42 R. S. Ruoff, T. D. Klots, T. Emilsson and H. S. Gutowsky, *J. Chem. Phys.*, 1990, **93**, 3142.
43 A. Zehnacker and M. A. Suhm, *Angew. Chem., Int. Ed.*, 2008, **47**, 6970.
44 F. Rondino, A. Ciavardini, M. Satta, A. Paladini, C. Fraschetti, A. Filippi, M. Speranza, A. Giardini and S. Piccirillo, *Rend. Fis. Acc. Lincei*, 2013, **24**, 259.
45 A. K. King and B. J. Howard, *J. Mol. Spectrosc.*, 2001, **38–42**, 205.

